ChemComm

COMMUNICATION

View Article Online
View Journal | View Issue

Cite this: *Chem. Commun.*, 2019, **55**, 1975

Received 8th November 2018,
Accepted 17th January 2019

DOI: 10.1039/c8cc08906j

rsc.li/chemcomm

Emission wavelength dependence on the rISC rate in TADF compounds with large conformational disorder†

Tomas Serevičius, *[a] Rokas Skaisgiris,[a] Jelena Dodonova,[b] Laimis Jagintavičius,[b] Jonas Bucevičius,[b] Karolis Kazlauskas,[a] Saulius Juršėnas[a] and Sigitas Tumkevičius[b]

Large vibronic coupling between the local and charge-transfer triplet states is required for efficient reverse intersystem crossing in TADF compounds. This is ensured by low steric hindrance between donor and acceptor molecular units. However, flexible molecular cores show large conformational disorder and emission wavelength instability in solid films.

According to the spin statistics, 75% of excitons formed in OLED devices are of non-emissive triplet nature, limiting their efficiency. Thermally activated delayed fluorescence (TADF) is the most promising pathway for triplet harvesting, since TADF compounds are cheaper and much more stable[1] than rare-earth metal based phosphorescent emitters widely used for display applications. Likewise, TADF OLEDs already show pronounced stability[2] and their external quantum efficiency (EQE) reaches exceptional values of about 40%[3] similar to the benchmark devices. All this makes TADF OLEDs perfect candidates to replace expensive phosphorescent OLEDs for applications in flat-panel screens and lighting in near future. The utilization of non-emissive triplet states in TADF emitters is achieved by thermally activated reverse intersystem crossing (rISC),[4] which is possible in molecular compounds with low singlet–triplet energy (ΔE_{ST}) gaps. Although several possible molecular geometries were suggested,[1,5] TADF emitters mostly are constructed from single-bonded donor (D) and acceptor (A) units. In such a geometry donor and acceptor units are twisted to nearly orthogonal angles[4,6] due to a steric hindrance ensuring a low overlap of π-electron orbitals in the HOMO and LUMO and sufficiently low ΔE_{ST}. However, steric hindrance between the D and A fragments should not be too large, as the strong restriction of twisting of the D–A fragments may reduce the vibronic coupling between localized (^{3}LE) and charge transfer (^{3}CT) triplet states, which is mandatory for efficient rISC,[7–9] and reduce the rISC rate. This requirement for a labile molecular core brings several interesting and unexpected effects. In dilute solutions, minor dispersion of D–A twist angles may be observed, having negligible effect on excited state relaxation. However, it becomes especially important in solid films, where molecules are frozen in conformations with a large variation of the molecular geometry. The existence of fixed molecular conformers in solid hosts causes the dispersion of ^{1}CT energies and ΔE_{ST} gaps, which has great importance in TADF properties.[10] There were several reports showing that conformational disorder of a molecular structure in solid hosts causes the temporal shifts of prompt and delayed fluorescence (PF and DF, respectively),[10–13] resulting in multiexponential DF decay with prolonged lifetime. However, the impact of conformational disorder on fluorescence properties, its relation to the rISC rate and methods to reduce the disorder, despite its importance, still are scarcely studied.

In this work we investigate the conformational disorder in solid films of phenothiazine–pyrimidine TADF compounds and its relation to emission properties. Compounds were designed to have different lability of the molecular structure and different reverse intersystem crossing (rISC) rate. A phenothiazine electron-donor unit was selected because of its ability to form several conformations, increasing the number of possible molecular structure arrangements in the solid state. We show that the variation of molecular structure rigidity of phenothiazine-pyrimidine compounds has only minor impact on conformational disorder and emission properties, while the rISC rate was found to have crucial importance in TADF properties.

The molecular structures and synthetic routes of phenothiazine–pyrimidine compounds **PTZ-mPYR**, **PTZ-mPYRCl** and **PTZ-2mPYR** are depicted in Scheme 1. Compounds **PTZ-mPYR** and **PTZ-mPYRCl**, designed to have different ISC and rISC rates by involving a heavy atom effect, were synthesized by Suzuki–Miyaura coupling of 4,6-dichloro-(**1a**) or 2,4,6-trichloropyrimidines (**1b**) with boronic acid **2** in the presence of $Pd(OAc)_2/PPh_3/Na_2CO_3$ as a catalyst system in 79% and 60% yields, respectively. Compound **PTZ-2mPYR**, designed to have a less labile molecular core than **PTZ-mPYR**, was synthesized

[a] *Institute of Photonics and Nanotechnology, Faculty of Physics, Vilnius University, Sauletekio 3, LT-10257 Vilnius, Lithuania. E-mail: tomas.serevicius@tmi.vu.lt*
[b] *Institute of Chemistry, Faculty of Chemistry and Geosciences, Vilnius University, Sauletekio 3, LT-10257 Vilnius, Lithuania*

† Electronic supplementary information (ESI) available: Synthesis, DFT calculations, CV data and details of photophysical characterization. See DOI: 10.1039/c8cc08906j

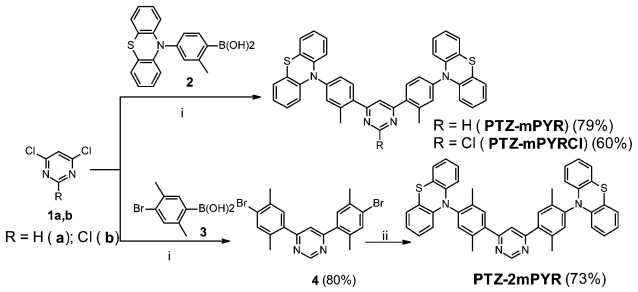

Scheme 1 The synthetic routes of **PTZ-mPYR**, **PTZ-mPYRCl** and **PTZ-2mPYR**. *Reagents and conditions*: (i) $Pd(OAc)_2$ (10 mol%), PPh_3 (20 mol%), Na_2CO_3 aq (6.2 equiv.), glyme/H_2O, Ar, 90 °C, 24 h; (ii) phenothiazine, $Pd(OAc)_2$ (5 mol%), P(*t*-Bu)$_3$·HBF_4 (10 mol%), NaO*t*-Bu (4 equiv.), toluene, Ar, 100 °C, 24 h.

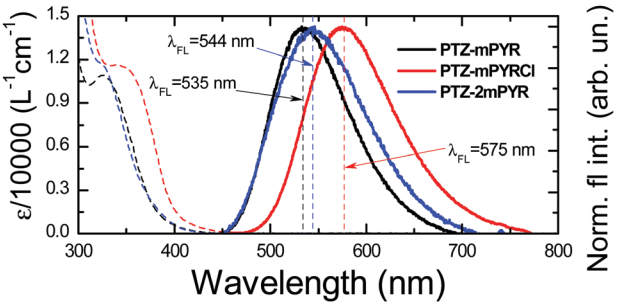

Fig. 1 Absorption and fluorescence spectra of the dominant $^1CT_{QE}$ band of phenothiazine–pyrimidine compounds in dilute toluene solutions. Excitation wavelength was 360 nm.

by a two-step protocol. Firstly, 4,6-dichloropyrimidine **1a** was coupled with boronic acid **3** to afford 4,6-bis(4-bromo-3,5-dimethylphenyl)-pyrimidine (**4**) in 80% yield. Then intermediate **4** was coupled with phenothiazine using the Buchwald–Hartwig amination reaction conditions to give the target **PTZ-2mPYR** in 73% yield. The synthetic details and characterization of the synthesized phenylboronic acids **2** and **3** and target compounds **PTZ-mPYR**, **PTZ-mPYRCl** and **PTZ-2mPYR** are presented in the ESI.†

Cyclic voltammetry analysis revealed that the energies of the HOMO were in the range of about −5.05 to −5.12 eV and those of the LUMO were in the range of −2.46 to −2.79 eV (see Fig. S1 and Table S1 in the ESI† for details).

DFT simulations were employed to optimize the molecular structure and estimate $S_0 \rightarrow S_n/T_n$ transition energies for different phenothiazine orientations (see Fig. S2 and Table S2 in the ESI†). Two main possible molecular conformations of a phenothiazine donor group[14–17] were found, when phenothiazine is oriented perpendicular (quasi-equatorial arrangement, QE) or parallel (quasi-axial arrangement, QA) to the bridging phenyl group. Only the QE conformer state was found for **PTZ-2mPYR** where the rotation of the phenothiazine unit was impeded by additional methyl groups (see Fig. S3 in the ESI†).[18,19] The total potential energies of all possible conformers differed by ∼30 meV (see Fig. S4 and Table S3 in the ESI†), thus all arrangements (including mixed QA–QE) may co-exist.[14,19,20] Different π-electron distribution patterns were found for QA, QA–QE and QE conformers. Low overlap of electron density in the HOMO and LUMO was found for QE conformers, while in QA conformations remarkable overlap was observed due to the low twist angle of the phenothiazine unit. QE and QE–QA conformers showed the lowest $S_0 \rightarrow S_1$ transition energies (∼2.56–2.98 eV) with negligible oscillator strengths (<0.001), however low ΔE_{ST} gaps up to 20 meV were estimated only for QE-oriented structures. QA conformers showed remarkably larger $S_0 \rightarrow S_1$ absorption energies (∼3.23–3.4 eV) with remarkably larger oscillator strengths (∼1.01) and ΔE_{ST} gaps of about 440 meV. TADF is expected only from QE conformers, while for QA states a negligible rISC rate is expected.

The absorption and fluorescence spectra of phenothiazine–pyrimidine compounds were analysed in dilute solutions and polymer films. The absorption and emission spectra in toluene are shown in Fig. 1. The absorption spectra showed a broad peak at 320–375 nm (with molar absorption coefficients of about 10^4 mol^{-1} cm^{-1}) of QA conformers (for compounds **PTZ-mPYR** and **PTZ-mPYRCl**) followed by a low intensity absorption band tail in the range of about 400–450 nm of QE states, typically for phenothiazine TADF compounds[14–17] and in-line with the DFT-predictions. The fluorescence spectra of $^1CT_{QE}$ states, after excitation with 360 nm light, peaked in the range of 544–575 nm. Broad and structureless spectra were of intramolecular charge-transfer (ICT) nature. Modification of phenyl fragments with methyl substituents enabled tuning of the FL peak energy for 40 meV due to varying HOMO–LUMO overlap (see Fig. S2 in the ESI†),[21] while the introduction of Cl atom redshifted the FL peak energy of 170 meV up to 575 nm for **PTZ-mPYRCl**.

The presence of different phenothiazine conformations, predicted by DFT simulations, was shown by measuring the fluorescence excitation spectra (see full fluorescence spectra in the log scale in Fig. S5 in the ESI†). Three distinct emission bands were observed for compounds **PTZ-mPYR** and **PTZ-mPYRCl** after excitation with 300–350 nm light: low intensity ^1LE (at about 300–400 nm) and $^1CT_{QA}$ (^1CT fluorescence from QA conformations) at about 400–450 nm together with very intense $^1CT_{QE}$ fluorescence (^1CT fluorescence of QE conformations) at 544–575 nm. Only $^1CT_{QE}$ emission was observed by exciting into the absorption tail at 410–450 nm. Other phenothiazine-based TADF compounds with a similar molecular structure also have shown fluorescence spectra composed of peaks from QA and QE conformers[14–16,22] and dominating $^1CT_{QE}$ emission. In contrast, only ^1LE and $^1CT_{QE}$ fluorescence peaks were observed for **PTZ-2mPYR** for all excitation wavelengths, when the formation of QA conformers was impeded by an extra methyl group.[22]

$^1CT_{QA}$ and $^1CT_{QE}$ emission peaks were also observed in the emission spectra of compounds **PTZ-mPYR** and **PTZ-mPYRCl** embedded in the PMMA host, while only $^1CT_{QE}$ emission was observed for **PTZ-2mPYR** (see Fig. 2a and b and Fig. S6 in the ESI,† black curves). Emission energies were slightly blueshifted in respect of toluene due to the lower dipole moment of PMMA. Singlet–triplet energy gaps between $^1CT_{QE}$ and ^3LE states were estimated to be in the range of 151–187 meV, small enough to observe thermally activated rISC[21] (see Fig. S7 in the ESI†). ΔE_{ST} gaps for QA conformers were too large for triplet upconversion. The presence of TADF was showcased by the temperature activation of delayed fluorescence (see Fig. S8 in the ESI†) and by comparing time-integrated fluorescence (TIFL) spectra in oxygen-sufficient (O_2^+) and deficient (O_2^-) ambient environments (see Fig. 2c and d and

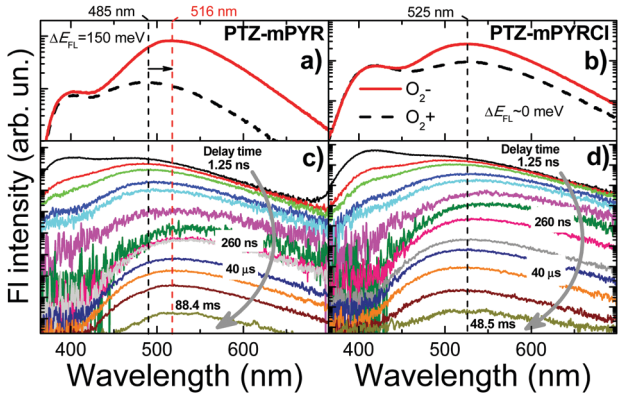

Fig. 2 (a and b) Time-integrated fluorescence spectra of 1 wt% PMMA films of **PTZ-mPYR** and **PTZ-mPYRCl**, respectively, in oxygen-sufficient (O_2^+, black lines) and oxygen-deficient (O_2^-, red lines) surroundings. (c and d) Time-resolved fluorescence spectra of 1 wt% PMMA films of **PTZ-mPYR** (c) and **PTZ-mPYRCl** (d) in O_2^- surrounding. Numbers close to Fl spectra denote delay times (1.25 ns for black lines, 260 ns for yellow lines, 40 µs for dark blue lines and 48.5/88.4 ms for the last spectrum). Vertical lines are guides for eyes.

Fig. S6 in the ESI†). TIFL intensity remarkably increased due to the weakened triplet state quenching by oxygen. Along with that, an unexpected effect was observed. The fluorescence peaks of compounds **PTZ-mPYR** and **PTZ-2mPYR** were redshifted for about 150 meV upon oxygen removal and TADF enhancement, while for **PTZ-mPYRCl** the emission peak energy remained the same.

The nature of such intriguing behaviour was revealed by analysing the temporal evolution of fluorescence spectra (see Fig. 2(c and d) and Fig. S6 in the ESI†). Emission peak energy was found to be time-dependent. Initially, the redshift was observed during the first 250–300 ns, followed by a blueshift later. The observed fluorescence shifts are caused by conformational disorder, the concept of which was elegantly introduced by Northey *et al.*[10] and experimentally observed by others.[11–13] Briefly, flexible donor–acceptor cores of TADF compounds are "frozen" in solid films with different twist angles between donor and acceptor fragments inducing the dispersion of ^{1}CT energies and ΔE_{ST} values. Conformations with the largest ^{1}CT energies have the largest oscillator strengths, and thus are expected to emit first, inducing a gradual redshift of PF. For DF, the opposite trend is observed due to exponential rISC rate dependence on ΔE_{ST}: conformations with the lowest ^{1}CT energies and smallest ΔE_{ST} gaps will emit first, inducing the gradual blueshift of TADF spectra. In our case, only $^1CT_{QE}$ fluorescence with pronounced CT characteristics was affected by conformational disorder. In ambient air (see Fig. S9 in the ESI†), the estimated redshift of the $^1CT_{QE}$ peak varied in the range of 280–380 meV (280 meV, 340 meV and 380 meV for **PTZ-mPYRCl**, **PTZ-mPYR** and **PTZ-2mPYR**, respectively), while the largest blueshift was estimated for **PTZ-mPYRCl** (110 meV) and for the rest of the compounds the blueshift was remarkably lower (40 meV for both **PTZ-mPYR** and **PTZ-2mPYR**). Under O_2^- conditions, the temporal evolution of prompt fluorescence was the same as in ambient air, however the delayed emission showed enhanced intensity at the latest delays (see Fig. S10 in the ESI†) followed by enlarged blueshift. The largest blueshift in ambient O_2^- was estimated for **PTZ-mPYRCl** (130 meV), which was almost the same as in ambient air. For **PTZ-mPYR** and **PTZ-2mPYR**, the blueshift was larger than in ambient O_2^+ (80 meV and 60 meV, respectively), however it still was markedly smaller than for **PTZ-mPYRCl**. In this way, the TIFL spectra of prompt and delayed emission peaked at different wavelengths in ambient O_2^+ and O_2^- for **PTZ-mPYR** and **PTZ-2mPYR**.

To find out why we observe a weaker blueshift for **PTZ-mPYR** and **PTZ-2mPYR** than that for **PTZ-mPYRCl**, fluorescence decay transients were analysed (see Fig. 3). Firstly, O_2^- toluene solutions were analysed in order to estimate the ISC and rISC rates. Double-exponential decay of prompt and delayed fluorescence at the $^1CT_{QE}$ peak was observed. TADF lifetime was comparable for **PTZ-mPYR** and **PTZ-2mPYR** (11 and 6 µs, respectively), while for **PTZ-mPYRCl** it was remarkably shorter, reaching 1.1 µs. Such short TADF lifetime is comparable to the benchmark values.[23] The most rapid TADF decay was followed by the largest delayed fluorescence/prompt fluorescence intensity (DF/PF) ratio of 1.2 for **PTZ-mPYRCl**, while for **PTZ-mPYR** and **PTZ-2mPYR** it was remarkably lower (0.3 and 0.03, respectively). TADF dominated in the emission of **PTZ-mPYRCl** while for **PTZ-mPYR** and **PTZ-2mPYR** the TADF intensity was lower despite almost the same ΔE_{ST} gaps. TADF enhancement in **PTZ-mPYRCl** was promoted by an internal heavy atom effect, enhancing spin–orbit coupling constant, crucial for intersystem crossing (ISC) and rISC.[24] The estimated TADF parameters are listed in Table S4 in the ESI.† The enhanced spin–orbit coupling for **PTZ-mPYRCl** resulted in the most rapid rISC rate, which reached 2×10^6 s^{-1}, about 12–17 times larger than for other compounds. The least efficient TADF for compound **PTZ-2mPYR** could be related to the restricted twisting of the phenothiazine donor fragment, which was shown to be the reason for a negligible rISC rate in similar phenothiazine-based TADF emitters[9] due to decreased coupling of ^{3}LE and ^{3}CT states, crucial for efficient TADF.[7]

Fluorescence decay transients of PMMA films at the dominant $^1CT_{QE}$ peak showed different properties as compared to

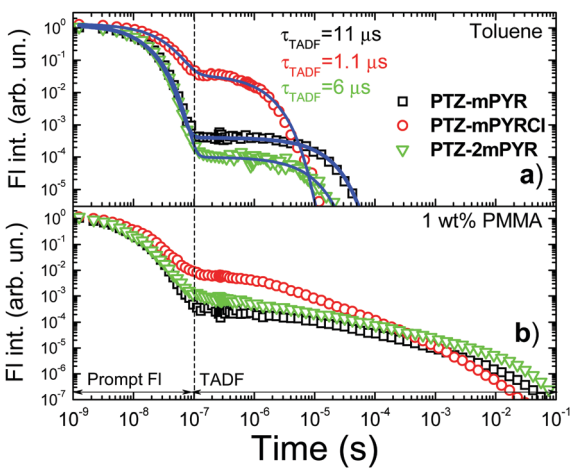

Fig. 3 Normalized $^1CT_{QE}$ fluorescence decay transients of phenothiazine–pyrimidine compounds in toluene (a) and 1 wt% PMMA films (b). Blue lines are biexponential fits.

dilute solutions. The decay of PF was rather typical however the DF decay was multiexponential with remarkably prolonged lifetime due to the conformational disorder. It resulted in tremendously enhanced DF/PF ratios of up to 33.5 (11.8, 8 and 33.5 for **PTZ-mPYR**, **PTZ-mPYRCl** and **PTZ-2mPYR**, respectively). Due to the multiexponential decay profile the TADF decay time and the rISC rate could hardly be correctly evaluated for compounds with such large conformational disorder, however it is clear that **PTZ-mPYRCl** still showed the most rapid TADF decay.

As we can see from the previous results, stable emission in PMMA films was observed for **PTZ-mPYRCl** with the fastest TADF decay. In this case, the TIFL spectra of delayed fluorescence in both ambient O_2^+ and O_2^- were very similar, thus no noticeable shift of the total TIFL spectrum after oxygen removal was observed. In contrast, the latest delayed fluorescence was missing for **PTZ-mPYR** and **PTZ-2mPYR** even under O_2^- conditions, which was completely suppressed by unknown quenchers. The lack of DF from the conformers with the largest ^{1}CT energy disturbed the high-energy shoulder of the TIFL spectrum, resulting in a redshift of its peak. Interestingly, the enhanced rigidity of the **PTZ-2mPYR** molecular core did not reduce the conformational disorder (for all compounds the redshift was rather comparable) and TIFL peak shift. Probably more sophisticated methods should be used to reduce the lability of such phenothiazine–pyrimidine cores. Another possible pathway to achieve low conformational disorder and stable emission wavelength for TADF compounds with slow TADF decay and flexible molecular cores is to use more rigid polymer or small-molecule hosts, impeding the conformation of molecular cores.[13]

In summary, three phenothiazine–pyrimidine TADF compounds with different molecular geometries were synthesized and comprehensively analysed by time-resolved spectroscopy. All compounds showed pronounced conformational disorder governing their emission properties. TADF efficiency and the rISC rate were altered by introducing heavy atoms due to enlarged spin–orbit coupling. A 150 meV redshift of the emission peak in solid films was observed after oxygen removal for compounds with a low rISC rate, while no shift was seen for compounds with rapid rISC. Such unusual behaviour was caused by the quenching of the long-lived DF bearing the largest ^{1}CT energy even in ambient O_2^-, resulting in the loss of the high-energy shoulder of TIFL spectra. Only minor quenching of the latest delayed emission and no noticeable shift of the TIFL spectrum were observed for compounds with rapid rISC. Our results showcase the importance of the large rISC rate in the TADF properties. We have shown that the emission energy of TADF compounds in solid films may depend not only on the conjugation length, but also on some unexpected parameters, such as the rISC rate or molecular core rigidity. This should be taken into account while designing novel TADF compounds.

This research was funded by a grant (No. S-MIP-17-73) from the Research Council of Lithuania. Regimantas Komskis is acknowledged for CV measurements. We are grateful to Dr Alytis Gruodis and High Performance Computing Center "HPC Sauletekis" in Vilnius University Faculty of Physics for total potential energy calculations.

Conflicts of interest

There are no conflicts to declare.

Notes and references

1 Y. Tao, K. Yuan, T. Chen, P. Xu, H. Li, R. Chen, C. Zheng, L. Zhang and W. Huang, *Adv. Mater.*, 2014, **26**, 7931–7958.
2 D. P.-K. Tsang, T. Matsushima and C. Adachi, *Sci. Rep.*, 2016, **6**, 22463.
3 T.-L. Wu, M.-J. Huang, C.-C. Lin, P.-Y. Huang, T.-Y. Chou, R.-W. Chen-Cheng, H.-W. Lin, R.-S. Liu and C.-H. Cheng, *Nat. Photonics*, 2018, **12**, 235–240.
4 H. Uoyama, K. Goushi, K. Shizu, H. Nomura and C. Adachi, *Nature*, 2012, **492**, 234–238.
5 T. Hatakeyama, K. Shiren, K. Nakajima, S. Nomura, S. Nakatsuka, K. Kinoshita, J. Ni, Y. Ono and T. Ikuta, *Adv. Mater.*, 2016, **28**, 2777–2781.
6 P. L. dos Santos, J. S. Ward, D. G. Congrave, A. S. Batsanov, J. Eng, J. E. Stacey, T. J. Penfold, A. P. Monkman and M. R. Bryce, *Adv. Sci.*, 2018, **5**, 1700989.
7 J. Gibson, A. P. Monkman and T. J. Penfold, *ChemPhysChem*, 2016, **17**, 2956–2961.
8 M. K. Etherington, J. Gibson, H. F. Higginbotham, T. J. Penfold and A. P. Monkman, *Nat. Commun.*, 2016, **7**, 13680.
9 J. S. Ward, R. S. Nobuyasu, A. S. Batsanov, P. Data, A. P. Monkman, F. B. Dias and M. R. Bryce, *Chem. Commun.*, 2016, **52**, 2612–2615.
10 T. Northey, J. Stacey and T. J. Penfold, *J. Mater. Chem. C*, 2017, **5**, 11001–11009.
11 G. Méhes, K. Goushi, W. J. Potscavage and C. Adachi, *Org. Electron.*, 2014, **15**, 2027–2037.
12 M. K. Etherington, F. Franchello, J. Gibson, T. Northey, J. Santos, J. S. Ward, H. F. Higginbotham, P. Data, A. Kurowska, P. L. Dos Santos, D. R. Graves, A. S. Batsanov, F. B. Dias, M. R. Bryce, T. J. Penfold and A. P. Monkman, *Nat. Commun.*, 2017, **8**, 14987.
13 T. Serevičius, T. Buciunas, J. Bucevičius, J. Dodonova, S. Tumkevicius, K. Kazlauskas and S. Jursenas, *J. Mater. Chem. C*, 2018, 11128–11136.
14 H. Tanaka, K. Shizu, H. Nakanotani and C. Adachi, *J. Phys. Chem. C*, 2014, **118**, 15985–15994.
15 P. L. dos Santos, J. S. Ward, A. S. Batsanov, M. R. Bryce and A. P. Monkman, *J. Phys. Chem. C*, 2017, **121**, 16462–16469.
16 M. K. Etherington, F. Franchello, J. Gibson, T. Northey, J. Santos, J. S. Ward, H. F. Higginbotham, P. Data, A. Kurowska, P. L. Dos Santos, D. R. Graves, A. S. Batsanov, F. B. Dias, M. R. Bryce, T. J. Penfold and A. P. Monkman, *Nat. Commun.*, 2017, **8**, 14987.
17 R. Huang, J. S. Ward, N. A. Kukhta, J. Avó, J. Gibson, T. Penfold, J. C. Lima, A. S. Batsanov, M. N. Berberan-Santos, M. R. Bryce and F. B. Dias, *J. Mater. Chem. C*, 2018, **6**, 9238–9247.
18 C. Chen, R. Huang, A. Batsanov, P. Pander, Y.-T. Hsu, Z. Chi, F. Dias and M. R. Bryce, *Angew. Chem., Int. Ed.*, 2018, **57**, 16407–16411.
19 K. Wang, C.-J. Zheng, W. Liu, K. Liang, Y.-Z. Shi, S.-L. Tao, C.-S. Lee, X.-M. Ou and X.-H. Zhang, *Adv. Mater.*, 2017, **29**, 1701476.
20 K. Wang, Y.-Z. Shi, C.-J. Zheng, W. Liu, K. Liang, X. Li, M. Zhang, H. Lin, S.-L. Tao, C.-S. Lee, X.-M. Ou and X.-H. Zhang, *ACS Appl. Mater. Interfaces*, 2018, **10**, 31515–31525.
21 R. Komatsu, T. Ohsawa, H. Sasabe, K. Nakao, Y. Hayasaka and J. Kido, *ACS Appl. Mater. Interfaces*, 2017, **9**, 4742–4749.
22 H. F. Higginbotham, C.-L. Yi, A. P. Monkman and K.-T. Wong, *J. Phys. Chem. C*, 2018, **122**, 7627–7634.
23 Y. Im, M. Kim, Y. J. Cho, J.-A. Seo, K. S. Yook and J. Y. Lee, *Chem. Mater.*, 2017, **29**, 1946–1963.
24 Y. Xiang, Y. Zhao, N. Xu, S. Gong, F. Ni, K. Wu, J. Luo, G. Xie, Z.-H. Lu and C. Yang, *J. Mater. Chem. C*, 2017, **5**, 12204–12210.

